Supportive Information

Two-step chemolytic delamination and depolymerization of multilayer laminated packaging films into valuable chemicals

Kalsoom Jan[a,b], Taofeng Lu[a], Christian Ayafor[c], Yuanqiao Rao[d], Junho Jeon[e], Junsi Gu[d], Maria C. Folgueras[d], Hsi-Wu Wong[f], and Wan-Ting Chen[a*]

[a]Department of Plastics Engineering, University of Massachusetts Lowell, Lowell, MA, USA. 01854

[b]Department of Chemistry, University of Massachusetts Lowell, Lowell, MA, USA. 01854

[c]Energy Engineering Program, University of Massachusetts Lowell, Lowell, MA, USA. 01854

[d]Core Research & Development, The Dow Chemical Company, Collegeville, PA, USA. 19426

[e]Core Research & Development, The Dow Chemical Company, Lake Jackson, TX, USA. 77566

[f]Department of Chemical Engineering, University of Massachusetts Lowell, Lowell, MA, USA. 01854

*Corresponding author: GraceWanTing_Chen@uml.edu

Number of Pages: 13

Number of Figures: 12

Number of Tables: 9

Table of Contents:

Section 1

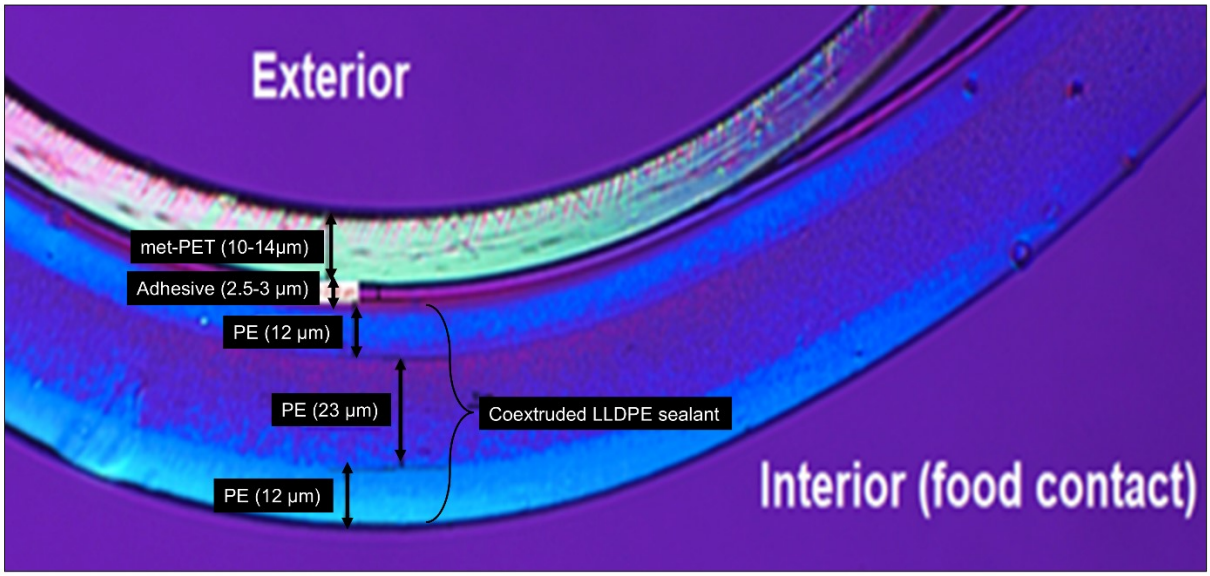

Fig. S1 Optical microscopy image of MLPF film used for two-step chemolysis

Section 2

Table S1 Hansen solubility parameters of solvents from literature

	Solvent	**δD**	**δP**	**δH**
Target	Acetic acid	14.5	8	13.5
Adjacent solvent	Iso-octyl alcohol	14.4	7.3	12.9
Target	Formic acid	14.6	10	14
Adjacent solvents	N-Butyl propionate	15.7	5.5	5.9

Note: Table S1 lists common and safer solvents, adjacent to acetic acid or formic acid in the HSP space, which are predicted to dissolve any grades of polyurethanes as specified in Table S2.

Table S2 Hansen solubility parameters of PUR from literature[1, 2]

Polymer name	**δD**	**δP**	**δH**	**Radius (R_a)**
Polyurethane 1	18.1	9.3	4.5	8
Polyurethane 2	19.9	8.1	6	9.8
Polyurethane 3	18.7	9.6	9.9	8.2

Note 1: Three grades of polyurethanes are available in the literature and were used to screen common, potentially safer, and possibly effective solvents.

Section 3

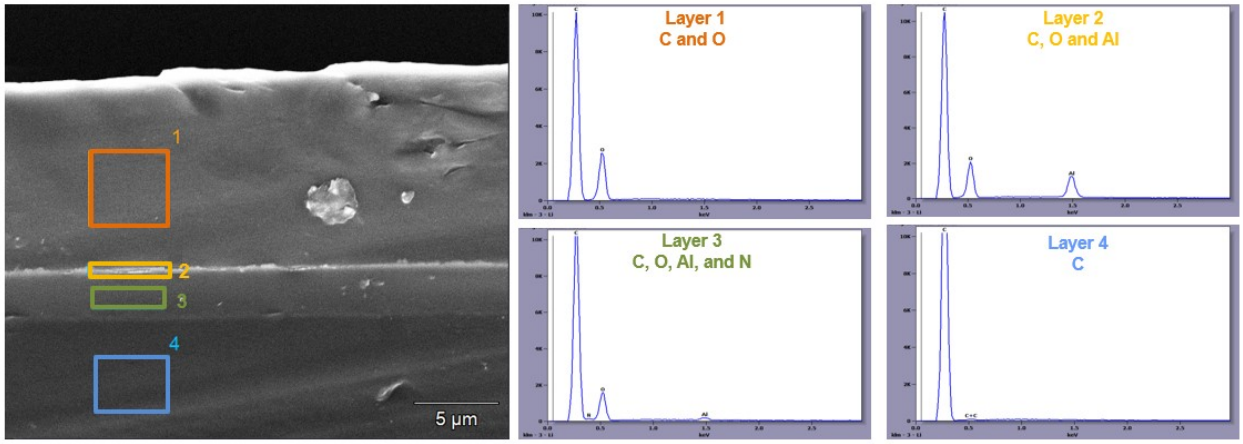

Fig. S2. SEM-EDS results of the MLPF used for delamination

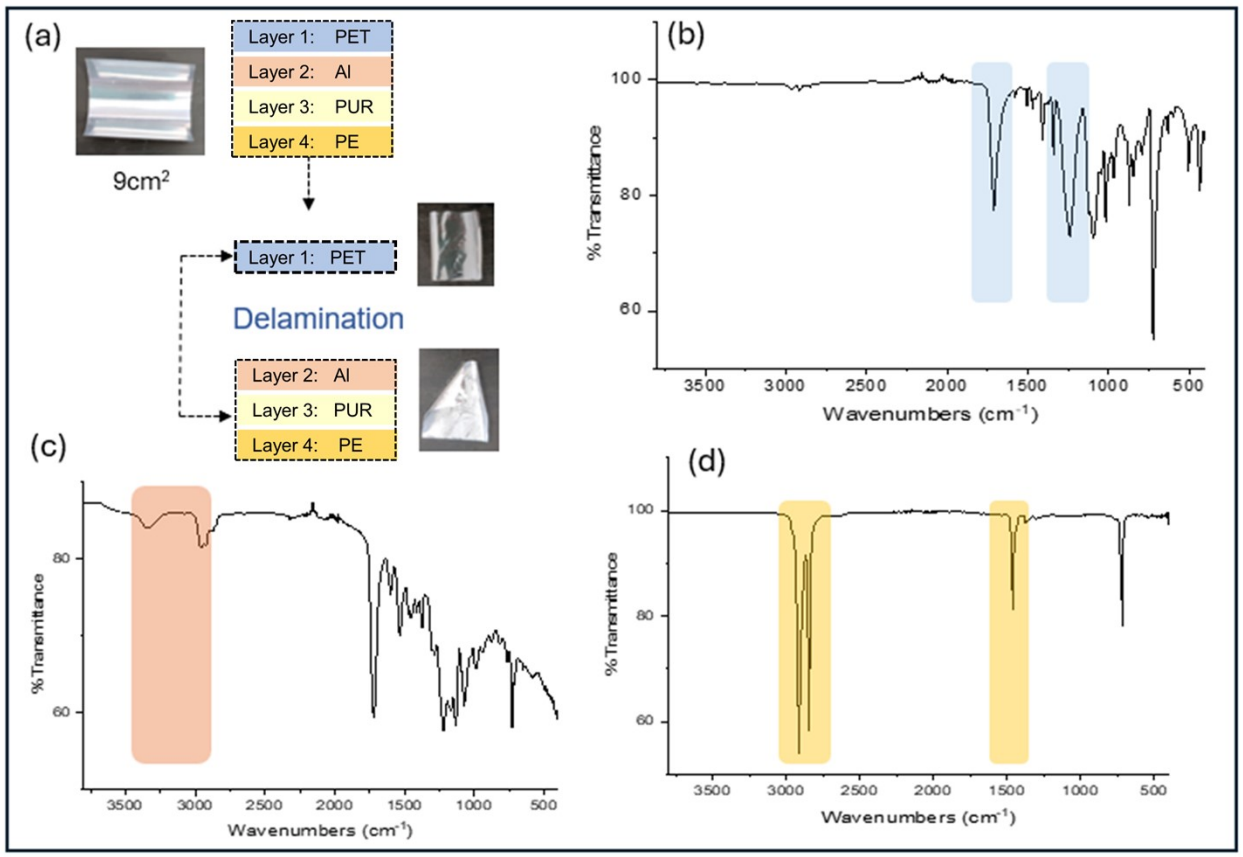

Fig. S3. FTIR analysis of the films after acidolysis: **(a)** the acidolysis scheme shows the delamination of the MLPF into individual components as PET and PUR//PE, **(b)** FTIR analysis of the delaminated PET film, which confirmed the purity of PET, **(c)** FTIR analysis of one side of the delaminated PUR//PE film, confirming the presence of the PUR-based adhesive, **(d)** FTIR analysis of the other side of the delaminated PUR//PE, showing the characteristic peaks of PE (note: it can be seen that the delaminated PUR//PE film still contains some aluminum, but this cannot be characterized by FTIR).

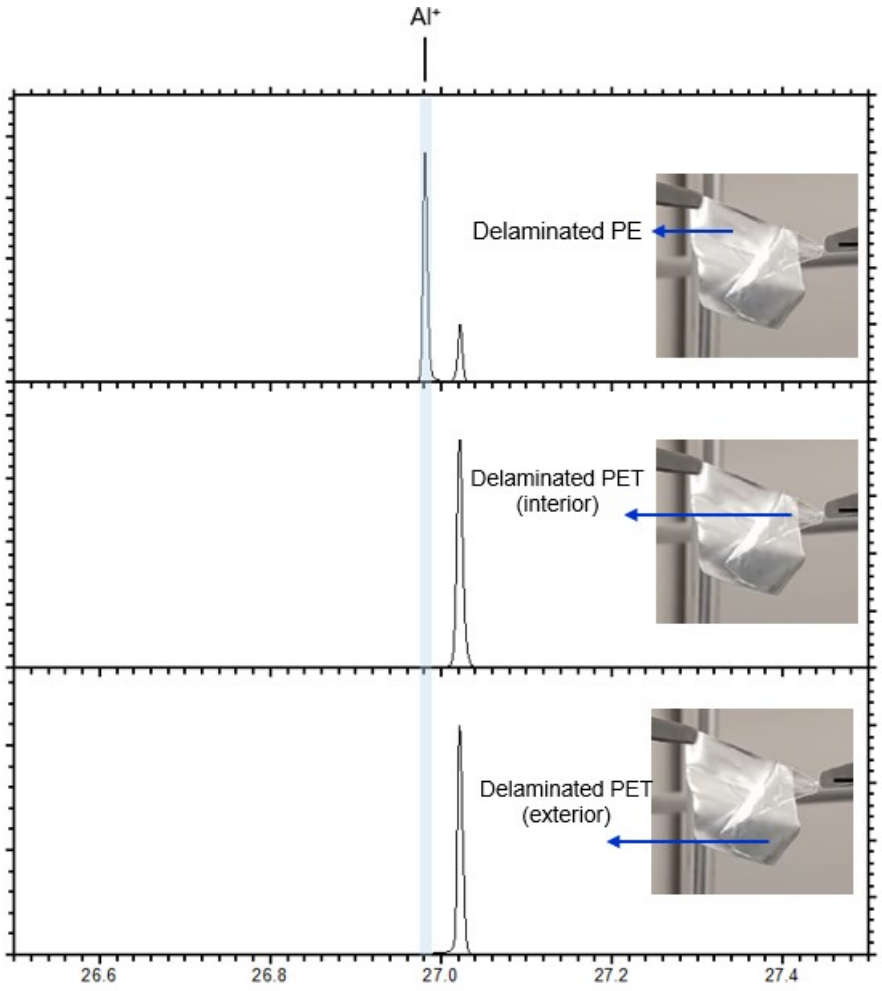

Fig. S4. Positive ion SIMS analysis to identify aluminum on the surface of (top) the delaminated PE layer (shiny surface, aluminum layer present), (middle) the interior side of the delaminated PET layer (transparent surface), and (bottom) the exterior side of the delaminated PET layer (transparent surface). Aluminum Al^+ at m/z 26.98 is highlighted in blue and is only observed on the surface of the delaminated PE layer. Insets show where each measurement was collected from in the MLPF structure.

Section 4

Table S3 Major compounds identified in the solution (obtained after delamination of MLPF in acetic acid) by using LC-MS

Compound Identified	Retention time (min)	[M+H]+ (m/z)
Ethyl N-(3-amino-2-methyl phenyl)carbamate	10.1	195.12
Ethyl N-(tosyl)carbamate	5.91	244.06
Ethyl N-[5-(ethoxy carbonyl amino)-2-methyl-phenyl]carbamate	9.8	267.16
Diethyl 4,4'-methylene bis(N-phenyl carbamate)	7.21	343.18
EDA-IPDI-6HHA	3.02	416.28

Table S4 GPC results of the PET film before and after acidolysis

	PET film before acidolysis	PET film after acidolysis
Mn (Dalton)	11904	11809
Mw (Dalton)	45297	44683
Mz (Dalton)	74887	73904
Mw/Mn	3.80	3.79

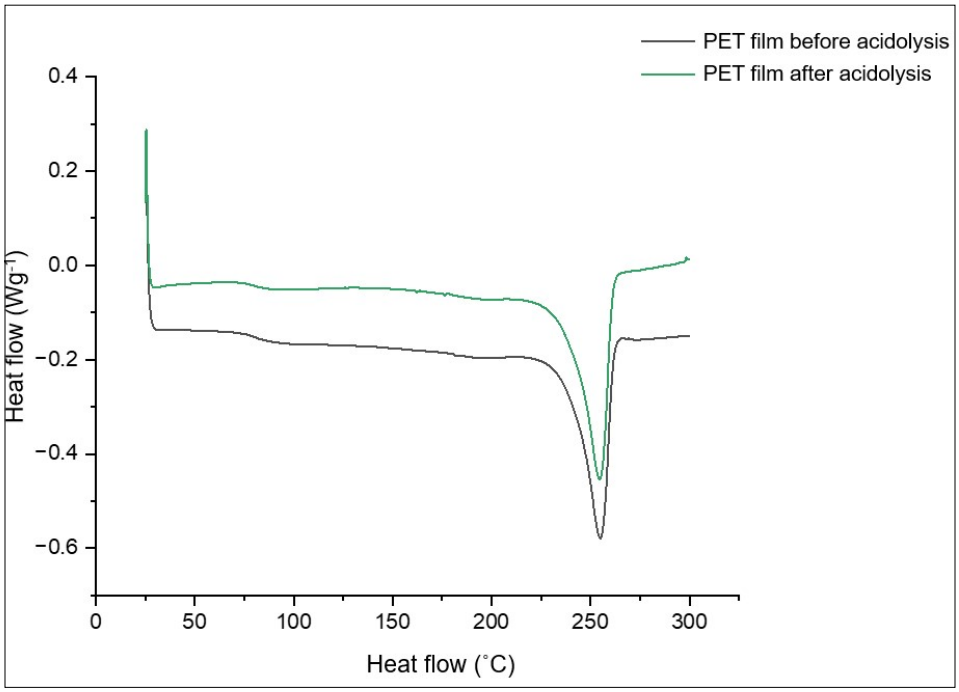

Fig. S5 DSC (2nd heating cycle) of the PET layer before and after acidolytic delamination (*n*=2)

Section 5

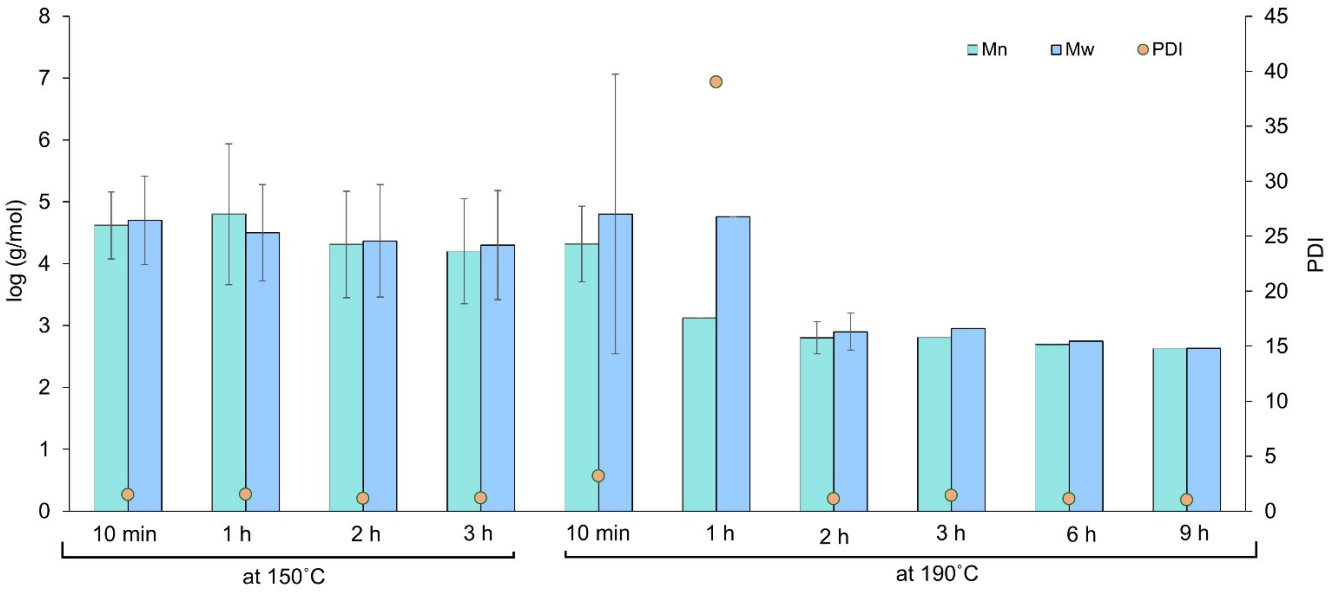

Fig. S6. GPC results of the product solutions obtained from the non-catalytic glycolysis of the delaminated PET films at different reaction times (note: *n*=2 except 1h and 3h-9h at 190˚C)

Section 6

Table S5. p-values (paired t-test, n ≥ 3) for selected comparisons in Fig. 6

Figure	Temperature	Comparison	P-value
6a (PET % Conversion)	170 °C	1 wt.% vs. 30 wt.%	0.0036
6a (PET % Conversion)	190 °C	1 wt.% vs. 30 wt.%	0.11
6a (PET % Conversion)	190 °C	1 wt.% vs. 5 wt.%	0.014
6b (BHET % Yield)	170 °C	1 wt.% vs. 30 wt.%	0.00074
6b (BHET % Yield)	190 °C	1 wt.% vs. 30 wt.%	0.0013

Table S6. p-values for PET conversion and BHET yield (n = 3)

Comparison	PET % Conversion	BHET % Yield
170 °C: 1 wt.% vs 30 wt.%	0.0056	0.066
190 °C: 1 wt.% vs 30 wt.%	0.15	0.0055
1 wt.%: 170 °C vs 190 °C	0.000027	0.00049
30 wt.%: 170 °C vs 190 °C	0.00092	0.000053

Table S7 Catalytic PET glycolysis using $Zn(OAc)_2$ at 190°C (*n*=2) at different reaction times

$Zn(OAc)_2$ wt. % loading	Reaction time (min)	PET % conversion	BHET %yield
0.3	30	5±3.1	-
0.3	90	99±0.61	97±0.42
0.003	30	0	-
0.003	120	98±0.34	96±0.87

Table S8 P-values (two-tailed t-test, n=3 comparing $Ca(OAc)_2{\cdot}H_2O$ (mono) and anhydrous $Ca(OAc)_2$

Metric	5 min	10 min	15 min
PET % conversion	0.57	0.33	N/A*
BHET % yield	0.00013	0.00014	0.00022

*For both $Ca(OAc)_2{\cdot}H_2O$ and anhydrous $Ca(OAc)_2$, PET conversion was 100% in all three replicates and thus the p-value is unavailable.

Section 7

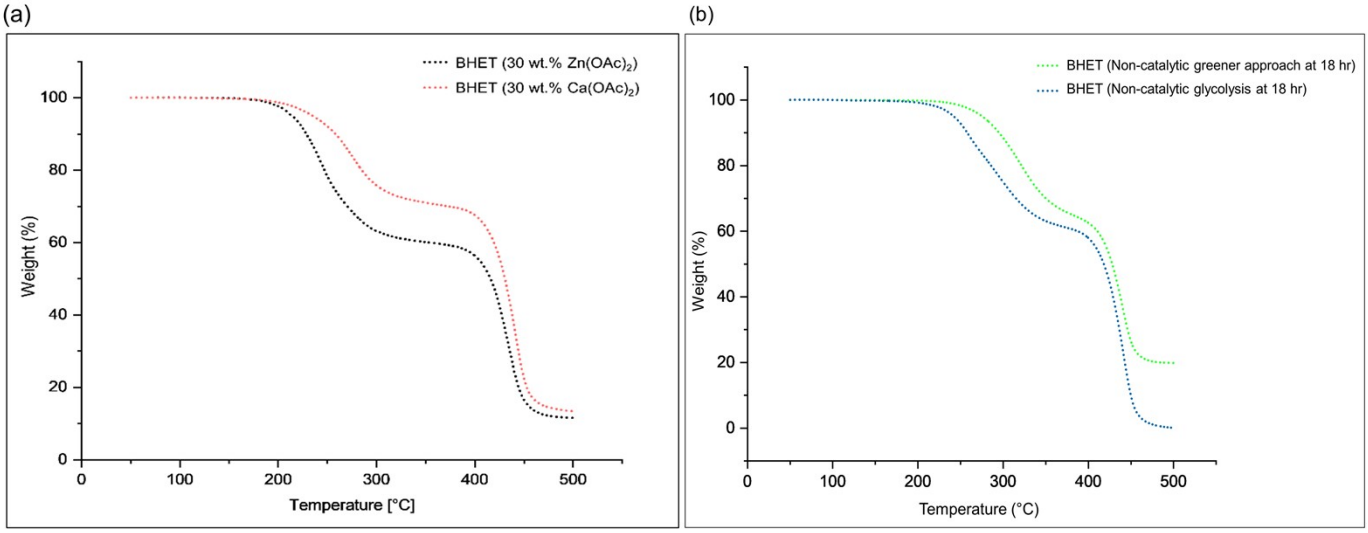

Fig. S7. TGA curves of the BHET obtained from **(a)** the catalytic glycolysis using 30 wt.% of $Zn(OAc)_2$ and $Ca(OAc)_2$ at 190°C and 10 min and **(b)** non-catalytic glycolysis of the delaminated PET films at 190˚C for 18 h

Section 8

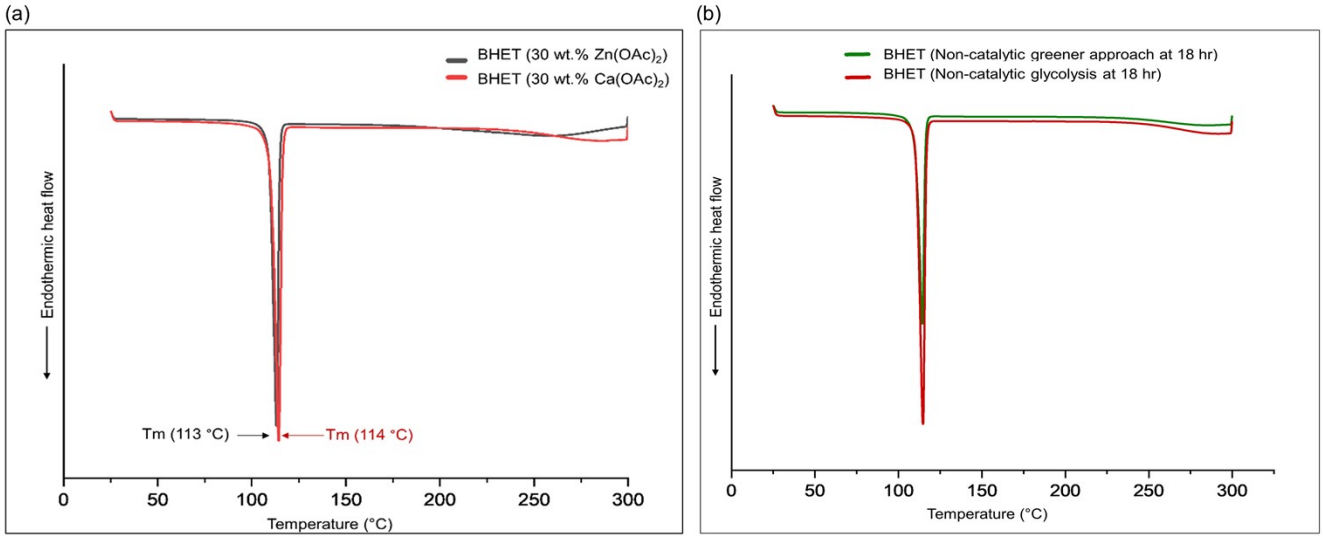

Fig. S8. DSC thermograms of **(a)** BHET obtained from catalytic glycolysis using 30 wt.% of Zn $(OAc)_2$ and Ca $(OAc)_2$ at 190°C and 10 min and **(b)** from non-catalytic glycolysis of the delaminated PET films at 190˚C for 18 h

Section 9

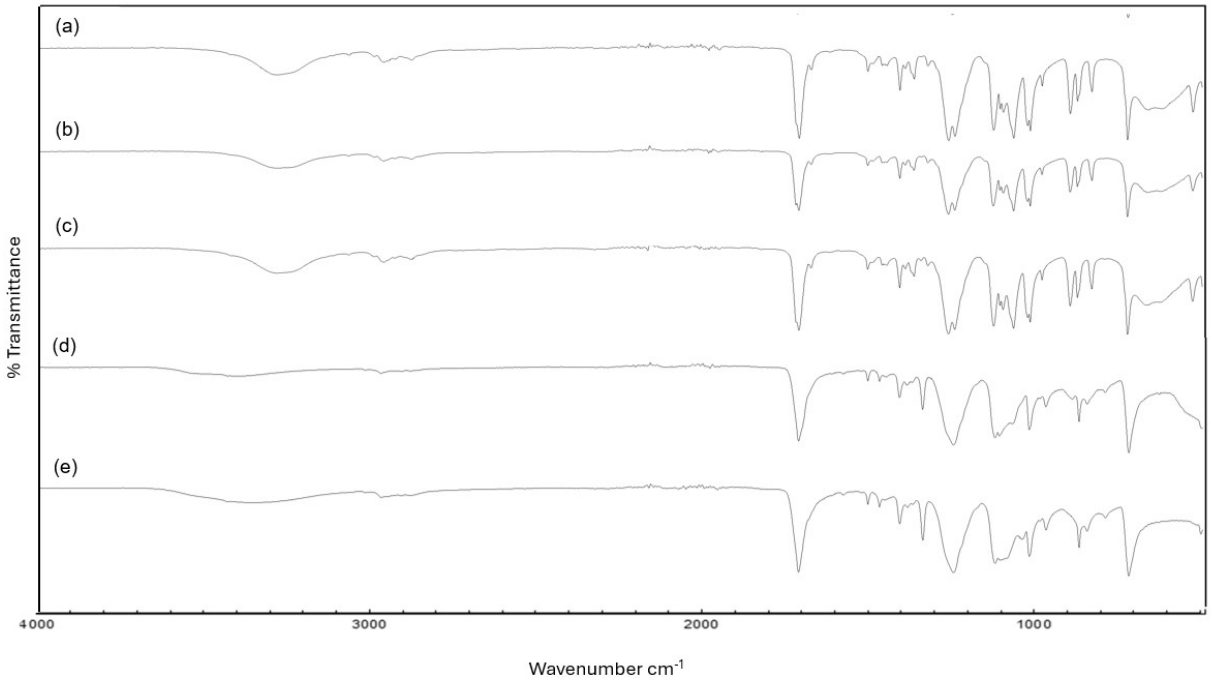

Fig. S9. FTIR spectra of BHET obtained from **(a)** non-catalytic glycolysis, **(b)** catalytic glycolysis using 30 wt.% $Zn(OAc)_2$, and **(c)** 30 wt.% $Ca(OAc)_2$, at 190°C and 10 min, as well as FTIR spectra of residual PET after reaction at 190°C from **(d)** non-catalytic glycolysis at 3 h and **(e)** catalytic glycolysis using 30 wt.% $Zn(OAc)_2$ after 1 min of reaction time

Section 10

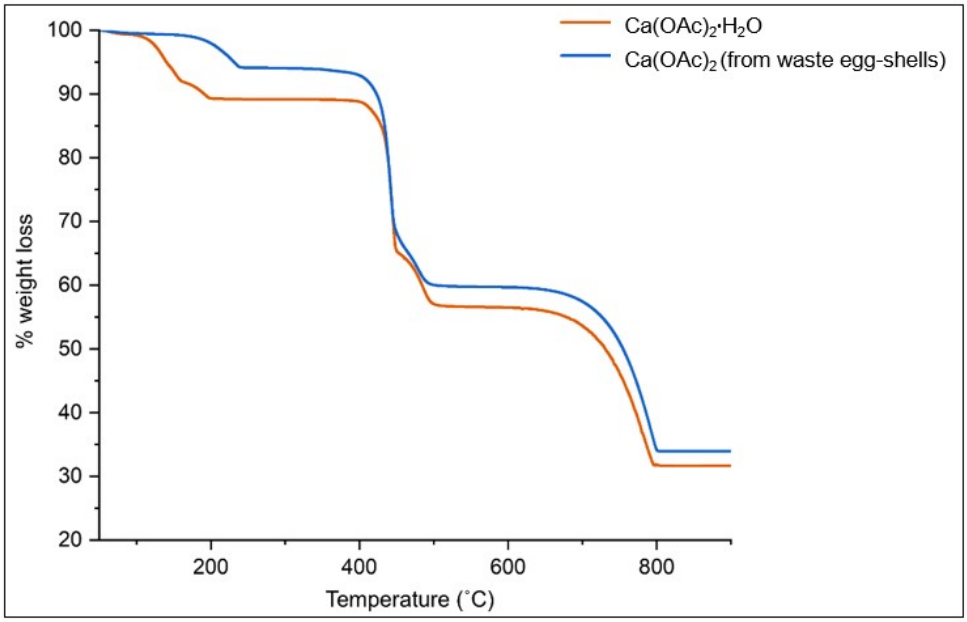

Fig. S10. Comparison of TGA thermograms of commercially available $Ca(OAc)_2 \cdot H_2O$ and anhydrous $Ca(OAc)_2$ synthesized from waste egg-shell

Section 11

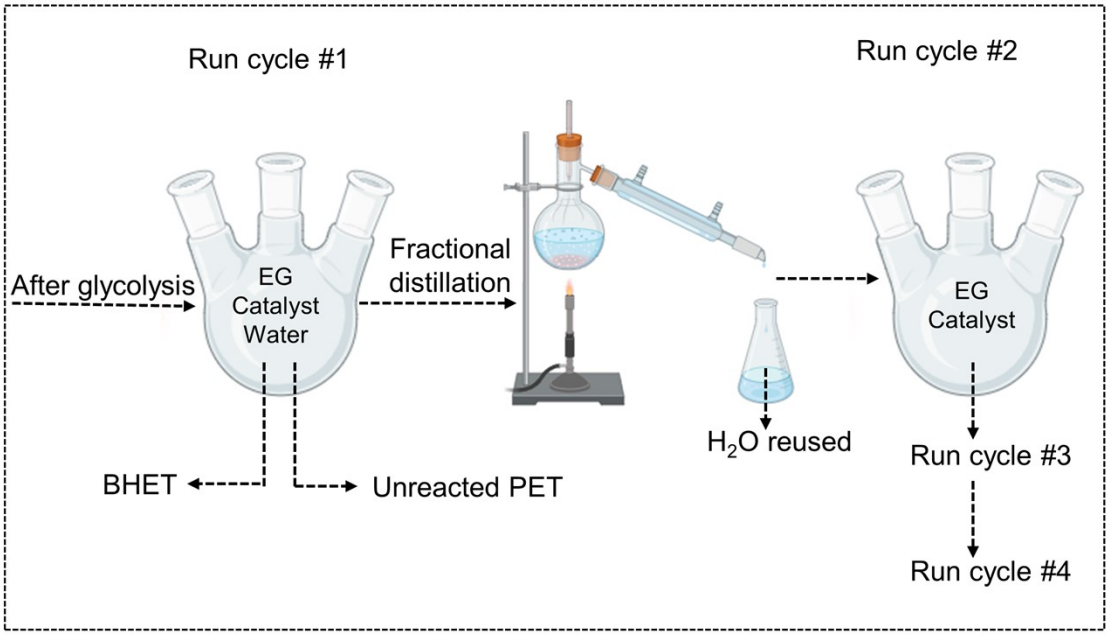

Fig. S11. The procedure for recycling and reusing the catalysts and EG for conducting multiple cycles of experiments

Section 12

Table S9. Compounds identified in the water recovered from fractional distillation (after glycolysis at 190°C-10 min)

$Zn(OAc)_2$ wt.% loading	Compound	Area
5 wt.%	Ethylene glycol	715899989
10 wt.%	Ethylene glycol	1227334833
30 wt.%	Ethylene glycol	993659163

Section 13

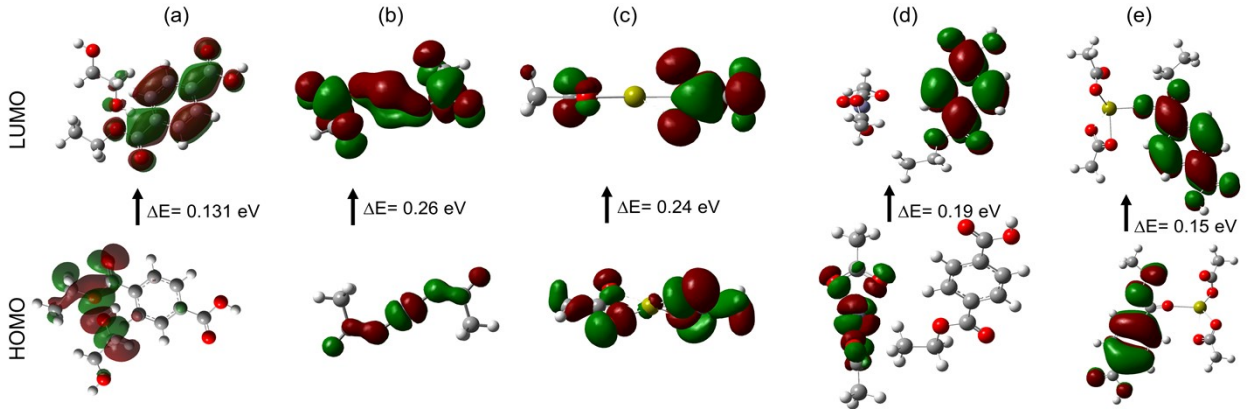

Fig. S12. Molecular orbitals (HOMO, LUMO) with energy gaps of **(a)** PET-EG, **(b)** $Zn(OAc)_2$, **(c)** $Ca(OAc)_2$, **(d)** PET-$Zn(OAc)_2$, and **(e)** PET-$Ca(OAc)_2$

References used in the Supportive Information:

1. C. H. Steven Abbott, and Yamamoto Hiroshi Hansen Solubility Parameters in Practice, https://www.hansen-solubility.com/HSPiP/, (accessed March 8, 2024).
2. C. M. Hansen, *Hansen solubility parameters: a user's handbook*, CRC press, 2002.